Accepted Manuscript

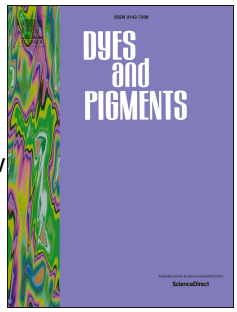

The role of electron-transporting Benzo[f]quinoline unit as an electron acceptor of new bipolar hosts for green PHOLEDs

Junseok Seo, So-Ra Park, Mina Kim, Min Chul Suh, Jihoon Lee

PII: S0143-7208(18)31967-3

DOI: https://doi.org/10.1016/j.dyepig.2018.11.024

Reference: DYPI 7168

To appear in: *Dyes and Pigments*

Received Date: 5 September 2018

Revised Date: 24 October 2018

Accepted Date: 11 November 2018

Please cite this article as: Seo J, Park S-R, Kim M, Suh MC, Lee J, The role of electron-transporting Benzo[f]quinoline unit as an electron acceptor of new bipolar hosts for green PHOLEDs, *Dyes and Pigments* (2018), doi: https://doi.org/10.1016/j.dyepig.2018.11.024.

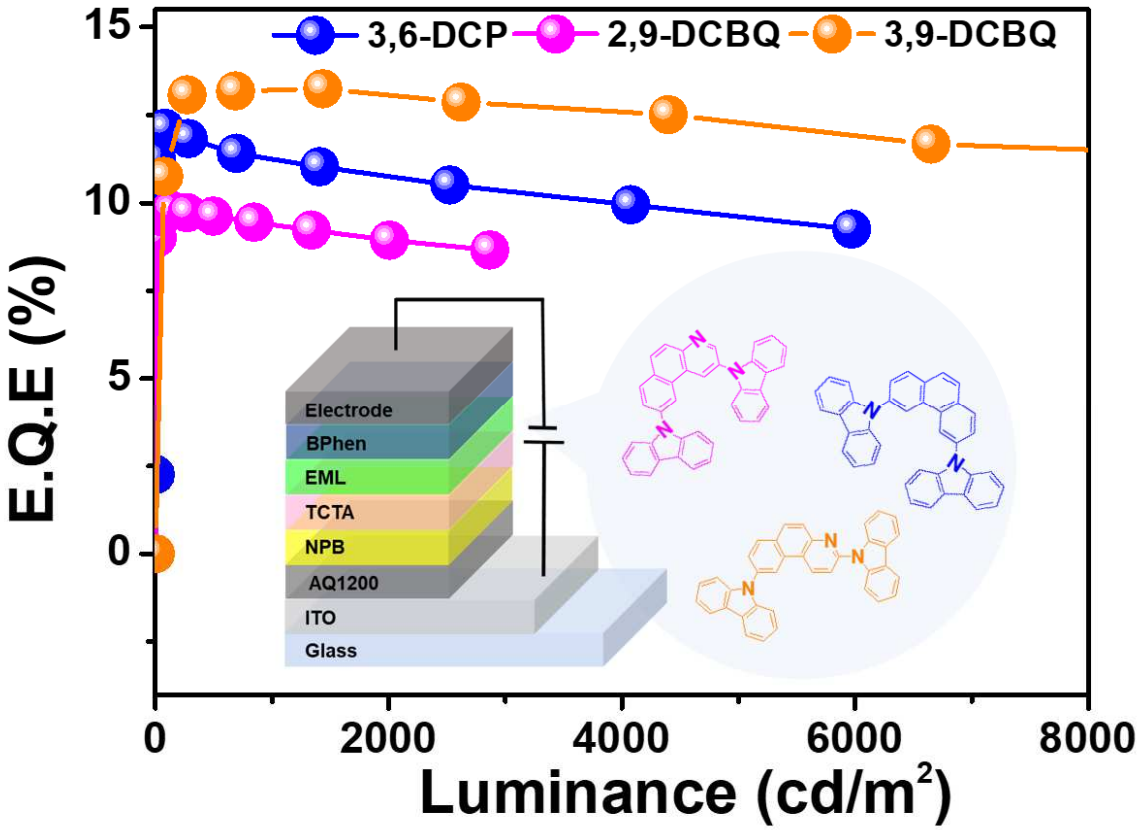

The Role of Electron-Transporting Benzo[f]quinoline Unit as an Electron Acceptor of New Bipolar Hosts for Green PHOLEDs

Junseok Seo[a,1], So-Ra Park[b,1], Mina Kim[a], Min Chul Suh[b,*], and Jihoon Lee[a,**]

[a] *Department of Polymer Science and Engineering & Department of IT Convergence (BK21 PLUS), Korea National University of Transportation, 50 Daehak-ro, Chungju, 27469, Republic of Korea*
[b] *Department of Information Display, Kyung Hee University, Dongdaemoon-Gu, Seoul 02447, Republic of Korea*

*Corresponding authors. Tel : +82-2-961-0694; Fax: +82-2-968-6924
E-mail: mcsuh@khu.ac.kr (Prof. M. C. Suh)
**Corresponding authors. Tel : +82-43-841-5427; Fax: +82-43-841-5420
E-mail: jihoonli@ut.ac.kr (Prof. J. H. Lee)
[1] Both authors have equally contributed to this work.

ABSTRACT

We prepared three new compounds [3,6-di(9H-carbazol-9-yl)phenanthrene (**3,6-DCP**), 2,9-di(9H-carbazol-9-yl)benzo[*f*]quinoline (**2,9-DCBQ**), and 3,9-di(9H-carbazol-9-yl)benzo[*f*]-quinoline (**3,9-DCBQ**)] containing phenanthrene or benzo[*f*]quinoline as an electron-withdrawing moiety and a carbazole as electron-donating moiety, respectively, as bipolar hosts for green phosphorescent organic light emitting diodes (PHOLEDs). We intentionally substituted nitrogen atom to the C-3 position of phenanthrene moiety to prepare benzo[*f*]quinolinegroup. And, we found that it allowed better electron transporting behavior than the phenanthrene moiety. Meanwhile, the benzo[*f*]quinoline/phenanthrene core moieties significantly improved the thermal stability of those host materials, which exhibited glass transition and decomposition temperatures of 132–139 and 395–427 °C, respectively. The green PHOLEDs which were fabricated with those host materials showed the lowest operating voltage of 4.7 V at 1000 cd/m^2 when we used **3,9-DCBQ**. Very interestingly, it has an asymmetric structure with completely separated HOMO and LUMO in space. In contrast, **3,6-DCP** having phenanthrene and carbazole moieties showed much higher operating voltage of 6.1 V which imply that replacing nitrogen at the C-3 position of phenanthrene improves carrier transport, that is, electron transporting behavior. As a result, the **3,9-DCBQ**-based PHOLED showed the best overall performance, exhibiting current and power efficiencies of 48.5 cd/A and 20.6 lm/W, respectively.

Keywords : green host materials, benzo[*f*]quinoline-based, photodehydrogenation, low operating voltage

1. Introduction

Organic light-emitting diodes (OLEDs) have been in the limelight of both academic and industrial research due to their highly efficient light emission and realization of outstanding colors. However, OLEDs suffer from reduced efficiency at high brightness, spurring extensive investigations aimed at mitigating this problem.[1] In particular, the low operating voltage and high thermal stability of OLEDs make them well-suited for display and illumination applications,[2, 3] with most of the corresponding phosphorescent hosts being of the bipolar type due to featuring an enhanced balance of electron and hole densities, wider recombination zone, lower operating voltage, and more simple device architecture.[4, 5] Generally, bipolar hosts comprise both electron donors (allowing hole transportation) and electron acceptors (allowing electron transportation), with carbazole being an example of the former class, and pyridine, triazine, imidazole, and cyano-substituted aromatics representing the latter one.[6-9] Herein, we describe the rational design of benzo[*f*]quinoline-based molecules to improve the thermal stability of hosts and replace previous electron-transporting materials. Among the numerous candidate substances, phenanthrene-based molecules enjoy the largest popularity, since their U-shaped structure suppresses close molecular packing and thus prevents crystallization. Moreover, the phenanthrene core can be regarded as a biphenyl derivative stitched in two *ortho*-positions by a short spacer and is thus expected to result in increased glass transition temperatures (T_g) and better thermal stability.[10, 11] Finally, the C-3 carbon of phenanthrene can be replaced by nitrogen, resulting in improved electron transportation. Fig. 1 shows the energy levels of the highest occupied molecular orbitals (HOMOs) and the lowest unoccupied molecular orbitals (LUMOs) of phenanthrene and its nitrogen-

containing analogues calculated by density functional theory (DFT) at the B3LYP level, revealing that the introduction of nitrogen decreased both HOMO and LUMO energies, with the exact magnitude of this decrease depending on the location of the N (nitrogen) atom. In fact, the exact position of the N atom required for improved performance is difficult to determine. However, the reduction of the LUMO energy without a significant change of molecular structure is certainly useful for improving the electron transport properties of hosts. In view of the above, we have synthesized three novel green PHOLED hosts, namely **3,6-DCP**, **2,9-DCBQ**, and **3,9-DCBQ**, as described in Scheme 1.

2. EXPERIMENTAL

2.1. General information.

All reagents and solvent were purchased from Sigma Aldrich and Alfa Aesar, TCI, Oakwood chem. All reactions were carried out under a N2 atmosphere. anhydrous toluene drying used the Molecular sieve (0.4 nm). The 1H and 13C nuclear magnetic resonance (NMR) was recorded on a Bruker 400MHz (Bruker DPX) NMR spectrometer. Ultraviolet-visible (UV-vis) spectrophotometer (HP8453) and fluorescence spectrophotometer (Perkin Elmer LS50B) were used to measure UV-vis spectra and photoluminescence (PL) spectra. Low-temperature PL measurement of the synthesized materials was carried out at 77 K using a dilute solution of the materials. Cyclic voltammetry (CV) were measured by a Autolab/PGSTAT 2 model, which was equipped with a platinum 3 array type as the working electrode, platinum wire as the counter electrode, and Ag/0.1M $AgNO_3$ as the reference electrode, at room temperature in a solution of tetrabuthylammonium hexafluorophospate (n-

Bu_4NPF_6)(0.1 N) in dimethyl formamide under nitrogen gas protection, at a scan rate of 100 or 50 mV/s. The differential scanning calorimeter (DSC) measurements was performed with a DSC2010 unit under a nitrogen flow at a heating rate of 10°C min-1. Thermogravimetric analysis (TGA) was conducted with a Thermogravimetric Analyzer S-1000 instrument under nitrogen with a heating rate of 10°C min-1 30 to 700°C. High resolution mass spectra were recorded using a HR-ESI MS SYNAPT G2 (Waters, U.K.) by the Ochang branch of the Korean Basic Science Institute.

2.2. Synthetic details

2.2.1. Synthesis of (4-bromobenzyl)triphenylphosphonium bromide (1). In a two-necked round bottom flask a mixture of 1-bromo-4-(bromomethyl)benzene (10 g, 40 mmol), triphenylphosphine (11.5 g, 44 mmol, 1.1 eq) in acetone (42 ml) was stirred at room temperature under N2 atmosphere for 12 h. The reaction mixture was then filtered and the white solids were collected washed with acetone before drying in vacuo (20.3 g, 99 %).

2.2.2. Synthesis of 1,2-bis(4-bromophenyl)ethene (2). A mixture of (4-bromobenzyl)triphenylphosphonium bromide (15 g, 29 mmol) and potassium tert-butoxide (3.45 g, 31 mmol, 1.05 eq) in THF (156 mL) was stirred in an ice-water bath for several minutes and then 4-bromobenzaldehyde (5.14 g, 28 mmol, 0.95 eq) was added. The solution was maintained at 0 ˚C and stirred continuously for a further 12 h. The mixture was then poured in water (100 mL) and extracted with dichloromethane (3 × 50mL). The organic

layer was washed with water (2 × 20 mL). The solution was concentrated under reduced pressure to obtain a viscous liquid, which was purified by column chromatography on silica gel and petroleum ether as eluent to give 1,2-bis(4-bromophenyl)ethene (6.7 g, 71 %). ^{1}H NMR (400 MHz, $CDCl_3$) δ (ppm): 7.48 (d, J = 8.5 Hz, 2H), 7.36 (dd, J = 8.4, 3.7 Hz, 4H), 7.14 – 7.00 (m, 3H), 6.54 (s, 1H).

2.2.3. Synthesis of 5-bromo-2-(4-bromostyryl)pyridine (3). Compound 3 was synthesized by the same procedure as described above for (1) using compound. Yield: 77 %; ^{1}H-NMR (400 MHz, $CDCl_3$) δ (ppm): 8.64 (d, J = 2.3 Hz, 1H), 7.79 (dd, J = 8.3, 2.4 Hz, 1H), 7.56 (d, J = 16.1 Hz, 1H), 7.50 (d, J = 8.5 Hz, 2H), 7.43 (d, J = 8.5 Hz, 2H), 7.28 (s, 1H), 7.09 (d, J = 16.0 Hz, 1H).

2.2.4 Synthesis of 2-bromo-6-(4-bromostyryl)pyridine (4). Compound 4 was synthesized by the same procedure as described above for (1) using compound. Yield: 76 %; ^{1}H NMR (400 MHz, $CDCl_3$) δ (ppm): 7.43 – 7.37 (m, 2H), 7.32 (d, J = 7.4 Hz, 2H), 7.17 (d, J = 8.4 Hz, 2H), 7.07 (d, J = 6.7 Hz, 1H), 6.77 (d, J = 12.5 Hz, 1H), 6.63 (d, J = 12.4 Hz, 1H).

2.2.5. Synthesis of 3,6-dibromophenanthrene (5). 1,2-bis(4-bromophenyl)ethene (4 g, 11.833 mmol), iodine (3.6 g, 14.2 mmol, 1.2 eq), THF (19.12 mL) and toluene (1 L) was irradiated using a 320 W HMPV lamp (300 nm) for 48 h/monitored by TLC. After the reaction was over, the excess of iodine was removed by washing the solution with aqueous $Na_2S_2O_3$, followed

by distilled water. The organic layer was concentrated under the reduced pressure. The pure product was isolated as a yellow solid by column chromatography over silica gel further crystallized from light petroleum ether (3.3 g, 83%). ^{1}H NMR (400 MHz, $CDCl_3$) δ (ppm): 8.72 (d, J = 1.7 Hz, 2H), 7.76 (d, J = 8.5 Hz, 2H), 7.74 – 7.68 (m, 4H).

2.2.6. Synthesis of 2,9-dibromobenzo[f]quinoline (6). Compound 6 was synthesized by the same procedure as described above for (5) using compound (3). Yield: 88 %; ^{1}H NMR (400 MHz, $CDCl_3$) δ (ppm): 9.00 (s, 2H), 8.68 (s, 1H), 7.96 (s, 2H), 7.86 – 7.74 (m, 2H).

2.2.7. Synthesis of 3,9-dibromobenzo[f]quinoline (7). Compound 7 was synthesized by the same procedure as described above for (5) using compound (4). Yield: 83 %; ^{1}H NMR (400 MHz, $CDCl_3$) δ (ppm): 8.74 – 8.69 (m, 2H), 7.96 (d, J = 3.6 Hz, 2H), 7.83 (d, J = 8.5 Hz, 1H), 7.77 (d, J = 8.5 Hz, 1H), 7.72 (d, J = 8.7 Hz, 1H).

*2.2.8. Synthesis of 3,6-di(9H-carbazol-9-yl)phenanthrene (**3,6-DCP**).* 3,6-dibromophenanthrene (1.6 g, 4.7 mmol), carbazole (1.65 g, 9.85 mmol, 2.07 eq), $Pd_2(dba)_3$ (0.28 g, 0.3 mmol), sodium *tert*-butoxide (0.91g, 9.5 mmol) and tri-*tert*-butylphosphine (50 wt% in toluene) (1.68 ml, 7.1 mmol, 1.5 eq) were charged to a flask. Then toluene (26 mL) was added to the flask, and the resulting mixture was stirred under N_2 at 90 ˚C overnight. The organic layer was extracted with toluene (2 × 30 mL) and dried over magnesium sulfate. The solvent was removed under reduced pressure, and the residue was purified by silica gel

column chromatography using CH_2Cl_2 / *n*-hexane (1:3) as the eluent. The resulting compound was obtained as a white powder (1.82 g, 75.6 %) and further purified by train sublimation in a 81.97 % yield. ^{1}H-NMR (400 MHz, CD_2Cl_2) δ (ppm) : 8.82 (d, J = 1.9 Hz, 2H), 8.23 (d, J = 8.4 Hz, 2H), 8.15 (dd, J = 7.7, 0.9 Hz, 4H), 8.01 (s, 2H), 7.88 (dd, J = 8.4, 2.0 Hz, 2H), 7.50 (d, J = 8.2 Hz, 4H), 7.39 (ddd, J = 8.3, 7.2, 1.2 Hz, 4H), 7.31 – 7.24 (m, 4H). ^{13}C-NMR (400 MHz, CD_2Cl_2) δ (ppm) : 141.37 136.71 131.68 131.45 130.95 127.45 126.60 126.52 123.79 121.36 120.69 120.53 110.04. HRMS (ESI) $[M+H]^+$: m/z calcd for $C_{38}H_{25}N_2$, 509.2018; found 509.1978.

*2.2.9. Synthesis of 2,9-di(9H-carbazol-9-yl)benzo[f]quinoline (**2,9-DCBQ**).* Compound 2,9-DCBQ was synthesized by the same procedure as described above for **3,6-DCP** using compound (6). Yield: 74.2 %; ^{1}H-NMR (400 MHz, CD_2Cl_2) δ (ppm) : 9.25 (d, J = 2.3 Hz, 1H), 9.10 (d, J = 2.3 Hz, 1H), 8.80 (d, J = 1.9 Hz, 1H), 8.30 (d, J = 8.5 Hz, 1H), 8.27 – 8.19 (m, 2H), 8.19 – 8.12 (m, 4H), 7.96 (dd, J = 8.4, 2.0 Hz, 1H), 7.54 – 7.45 (m, 4H), 7.45 – 7.36 (m, 4H), 7.35 – 7.25 (m, 4H). ^{13}C-NMR (400 MHz, CD_2Cl_2) δ (ppm): 149.65 147.88 141.29 137.29 132.66 131.18 128.86 127.33 126.78 126.60 126.14 124.05 123.87 121.04 120.86 120.75 120.69 109.97 109.73 HRMS (ESI) $[M+H]^+$: m/z calcd for $C_{37}H_{24}N_3$, 509.1892; found 510.1961.

*2.2.10. Synthesis of 3,9-di(9H-carbazol-9-yl)benzo[f]quinoline (**3,9-DCBQ**).* This compound was also synthesized by the same procedure as described above for **3,6-DCP** using compound (7). Yield: 75.3%; ^{1}H-NMR (400 MHz, CD_2Cl_2) δ (ppm): 9.06 (d, J = 8.7 Hz, 1H), 8.86 (d, J

= 1.8 Hz, 1H), 8.24 (d, J = 8.5 Hz, 1H), 8.22 – 8.18 (m, 3H), 8.17 – 8.11 (m, 3H), 8.11 – 8.07 (m, 2H), 7.94 (d, J = 8.8 Hz, 1H), 7.89 (dd, J = 8.4, 2.0 Hz, 1H), 7.57 – 7.52 (m, 2H), 7.51 – 7.47 (m, 2H), 7.46 – 7.42 (m, 2H), 7.36 (dd, J = 7.2, 0.9 Hz, 2H), 7.32 (dd, J = 7.0, 0.9 Hz, 2H). ^{13}C-NMR (400 MHz, CD_2Cl_2) δ (ppm): 151.77 148.56 141.45 139.94 137.25 134.12 131.64 131.26 131.08 126.72 126.60 126.56 124.9 123.90 121.7 121.20 120.79 120.67 120.56 117.79 112.16 110.12 HRMS (ESI) $[M+H]^+$: m/z calcd for $C_{37}H_{24}N_3$, 509.1892; found 510.1959.

2.3. Device fabrication and measurement

2.3. 1. Materials

We purchased or synthesized the following materials. Plexcore® OC AQ1200 (AQ1200) was purchased from Sigma-Aldrich as hole injection layer (HIL). N,N′-bis(naphthalen-1-yl)-N,N′-bis(phenyl)benzidine (NPB) and tris(4-carbazoyl-9-ylphenyl) amine (TCTA) were purchased from Lumtec Corp. and used as a hole transport layer (HTL) as well as exciton blocking layer (EBL), respectively. **3,6-DCP**, **2,9-DCBQ** and **3,9-DCBQ** were synthesized and utilized as host materials for emitting layer (EML). Bis(2-phenylpyridine)(acetylacetonato) iridium (III) [$Ir(ppy)_2(acac)$] was purchased from Lumtec Corp. and used as a phosphorescent green dopant for the EML. 4,7-diphenyl-1,10-phenanthroline (BPhen) as an electron transport layer (ETL), lithium fluoride (LiF) as the materials for an electron injection layer (EIL), and aluminum (Al) as a cathode were also purchased from the commercial suppliers and were used without purification.

2.3. 2. Decvie fabrication

To fabricate OLED devices, a 150 nm thick patterned indium-tin oxide (ITO) glasses with an open emission area of 4 mm^2 were used. The ITO glasses were cleaned in acetone and isopropyl alcohol with sonication process and rinsed in deionized water. Then, ITO glass substrates were treated in UV-ozone system to eliminate all the organic impurity remained during previous fabrication processes. AQ1200 was spin-coated on ITO glass in ambient condition and annealed at 120 ^oC for 15min in the nitrogen atmosphere. Subsequently, all the organic materials were deposited on AQ1200 by vacuum evaporation technique under a pressure of ~$1x10^{-6}$ Torr. The deposition rate of organic layers was about 0.5 Å/s. LiF and Al were deposited with rates of 0.1 Å/s and 3 Å/s, respectively. The current density-voltage (*J-V*) and luminance-voltage *(L-V*) data of OLEDs were collected by Keithley SMU 2635A and Minolta CS-100A, respectively. Electroluminescence (EL) spectra and the Commission Internationale De'Eclairage (CIE) coordinates were obtained using a Minolta CS-2000A spectroradiometer.

3. Results and discussion

3.1. Synthesis

The synthesis and structures of PHOLED hosts are shown in **Scheme 1**. Compound **1** was prepared via the phosphine alkylation,[12, 13] and **2**–**4** were synthesized via Wittig reactions, which, however, always produce *E/Z* isomers in a 1:1 ratio.[14, 15] Intermediates **5**, **6**, and **7** were prepared via photodehydrogenation using a 320-W high-pressure mercury vapor lamp

(3000 Å). During the above photoreaction, the *E*/*Z*-isomers were interconverted, with the subsequent cyclization shifting the equilibrium to the desired side.[16-18] Finally, Buchwald Hartwig coupling[19] afforded the desired hosts, with their overall yields over four steps equaling ~48 %. The identities of all compounds were confirmed by ^{1}H and ^{13}C nuclear magnetic resonance spectroscopy and electrospray ionization mass spectrometry.

3.2. Photophysical properties

The UV-vis absorption and PL spectra of the above hosts in toluene are shown in Fig. 2 and summarized in Table 1. Despite the shapes of UV-vis absorption peaks being slightly different for each host, they corresponded to traditional carbazole absorption wavelengths, with the related absorption maxima (assigned to n-π* transitions) located at 340 nm (**3,6-DCP** and **2,9-DCBQ**) and 374 nm (**3,9-DCBQ**).[20] The corresponding PL maxima were located at 388, 401, and 396 nm for **3,6-DCP**, **2,9-DCBQ**, and **3,9-DCBQ**, respectively, being slightly red-shifted by 6-13 nm in the case of thin films. Thus, the intermolecular interaction was significantly suppressed when carbazole moieties were attached to the rigid core that hindered close molecular packing. The optical bandgap energies (E_g^{opt}) of **3,6-DCP**, **2,9-DCBQ**, and **3,9-DCBQ** were determined from their absorption edges (λ_{cutoff}) as 3.29, 3.04, and 3.20 eV, respectively, with the corresponding triplet energies (E_T) determined from phosphorescence spectra at 77 K as 2.56, 2.60, and 2.62 eV, respectively, exceeding that of $Ir(ppy)_2(acac)$ (2.47 eV) and indicating that the $Ir(ppy)_2(acac)$-to-host triplet energy transfer was completely suppressed.[21]

3.3. Thermal properties

The thermal properties of the hosts were investigated by TGA and DSC in an atmosphere of nitrogen, which revealed that all compounds showed relatively high grass-transition temperature (T_g) and decomposition temperature (T_d) (Fig. 3 and Table 1). Temperatures corresponding to 5% weight loss were determined by TGA as 402 °C (**3,6-DCP**), 395 °C (**2,9-DCBQ**), and 427 °C (**3,9-DCBQ**), with DSC measurements revealing T_g's of 132 °C for **3,6-DCP** and 139 °C for **2,9-DCBQ** and **3,9-DCBQ**. Both phenanthrene and benzo[*f*]quinoline exhibit a rigid flat structure and are thus regarded as compounds with outstanding thermal stability. DFT-based calculations showed that the dihedral angles between the phenan-threne/benzo[*f*]quinoline core and carbazole side groups were in the range of 42.1–53.6° (Fig. S1). This might be related to how T_m was not observed in the 2nd scan as molecules were not piled on the solid form. The three synthesized hosts exhibited an almost two-fold increased T_g's compared to that of a typical green host material, 4,4′-bis(*N*-carbazolyl)-1,1′-biphenyl (**CBP**) (62 °C).

3.4. Theoretical calculations

The electronic structure of the hosts was further investigated by quantum chemical calculations using the Materials Studio 7.0 D-Mol3 software package and the density functional theory (DFT) calculations at the Lee-Yang-Parr correlation (B3LYP) level of theory, with the above dihedral angles determined as 53.6° (C11-C12-N28-C29 for **3,6-DCP**), 51.0° (C11-C12-N42-C43 for **2,9-DCBQ**), and 42.1° (C12-C13-N16-C21 for **3,9-DCBQ**) (Fig. 4 and Fig. S1). The twisted geometry of these hosts effectively prevented close

molecular packing in the solid state and thus suppressed recrystallization and improved film stability. The HOMO of **3,9-DCBQ** was localized on the carbazole ring located further away from the nitrogen of the benzo[*f*]quinoline core, whereas the corresponding LUMO was localized on the core, achieving complete spatial HOMO-LUMO separation and thus realizing bipolar charge transportation. In contrast to the above example, the HOMOs of **3,6-DCP** and **2,9-DCBQ** featured non-zero contributions of the core, with the corresponding LUMOs being localized on phenanthrene and benzo[*f*]quinoline, respectively. In other words, the spatial HOMO-LUMO separation was determined by the asymmetrical or pseudo-symmetrical molecular structure. In pseudo-symmetrical hosts (**3,6-DCP** and **2,9-DCBQ**), the electron density of HOMO is broadly distributed from both carbazole units through core unit, while electron density of LUMO is being localized only on the core moiety. Conversely, the HOMO of the asymmetrical **3,9-DCBQ** was localized only on the carbazole ring located further away from the N atom of the benzo[*f*]quinoline core, resulting in complete spatial separation. The reason why this difference arises is that the conjugation between the core moiety and the right carbazole moiety in **3,9-DCBQ** is more efficient than that of **3,6-DCP** and **2,9-DCBQ**, so that the core moiety and the right carbazole moiety behave like one unit (electron transport unit) . On the other hand, since the carbazole on the left side is bent more than 50 degrees, it can be considered that it will not share the electron density with the core unit. This might help to separate the each carrier pathway for efficient charge transportation and recombination. Notably, the substitution of phenanthrene for benzo[*f*]quinoline effectively lowered the HOMO and LUMO energies of host molecules. From this change, the electron energy barrier between BPhen and EML is reduced, and current injection could be enhanced.

3.5. Device characteristics

To verify the design concept of new synthetic host materials, we prepared green PHOLEDs as follows (see also Fig. 5):

Device A: ITO / AQ1200 (40 nm) / NPB (30 nm) / TCTA (10 nm) / **3**,**6-DCP** : $Ir(ppy)_2(acac)$ (20 nm, 3 wt.%) / BPhen (50 nm) / LiF (1 nm) / Al (100 nm)

Device B: ITO / AQ1200 (40 nm) / NPB (30 nm) / TCTA (10 nm) / **2**,**9-DCBQ** : $Ir(ppy)_2(acac)$ (20 nm, 3 wt.%) / BPhen (50 nm) / LiF (1 nm) / Al (100 nm)

Device C: ITO / AQ1200 (40 nm) / NPB (30 nm) / TCTA (10 nm) / **3**,**9-DCBQ** : $Ir(ppy)_2(acac)$ (20 nm, 3 wt.%) / BPhen (50 nm) / LiF (1 nm) / Al (100 nm)

Fig. 6(a) shows the *J-V-L* characteristics of the fabricated green PHOLEDs. The representative results are summarized in Table 2. At a given constant voltage of 5.0 V, the *J* values of 0.17, 0.37, and 2.90 mA/cm^2 were observed in the fabricated **Devices A**, **B**, and **C**, respectively. This is the result which was affected by the different electron injection barrier from ETL to EML as aforementioned as shown in Fig. 5. Turn-on voltages (V_{on}) of 4.0, 3.5, and 3.0 V were obtained from the **Device A**, **B,** and **C**, respectively. Meanwhile, the operating voltages (V_{op}) required to reach 1,000 cd/m^2 were 6.1, 6.6, and 4.7 V for the **Devices A**, **B,** and **C**, respectively. (see also Table 2). The maximum current efficiencies were 44.0, 35.5, and 48.5 cd/A for **Devices A**, **B**, and **C**, respectively. The maximum power efficiencies were 13.1, 12.3, and 20.6 lm/W, for **Device A**, **B**, and **C**, respectively. Those data were also summarized in Table 2. The maximum external quantum efficiency (EQE) values also increased in the order of **Device B** (9.8%) < **Device A** (12.1%) < **Device C** (14.3%), as

shown in **Fig. 6(b)**. From those results, we found that **Device C** (**3**,**9-DCBQ**) showed the greatest current density and better efficiency than the other **Devices**, which might be attributed to its improvement of electron affinity by substituting carbon for nitrogen (i.e., phenanthrene → benzoquinoline). However, **Device B** (**2**,**9-DCBQ**) showed lower the current density than **Device C** (**3**,**9-DCBQ**), despite they also have same benzoquinoline moiety, which might be due to the inefficient electron transporting characteristics originated from the difference in their molecular structure (i.e. symmetric and asymmetric).[22-24] In other words, since electron transport units (e.g. phenanthrene and benzoquinoline) in **3,6-DCP** and **2,9-DCBQ** have slightly occupied HOMOs which means that some hole carriers can also be transported through those moieties while they have completely vacant cabazole moiety in their LUMOs (e.g. electron can only be transported through those moieties). This might affect that the hole carriers transmitted through central moieties could impede an electron transport ability of those groups during operation. In contrast, the electron transport properties of **3,9-DCBQ** could be ideal because this molecule has completely separated HOMO and LUMO.

In addition, the charge trapping behavior of an electron and/or a hole strongly depends on the energy gap of HOMOs or LUMOs between the host and the dopant molecules. In our EML system [**3**,**6-DCP**, **2**,**9-DCBQ**, and **3**,**9-DCBQ** doped with $Ir(ppy)_2(acac)$] they show very deep hole trapping level while they show very shallow and negligible electron trapping level, as shown in Fig. 5. As a result, an exciton recombination zone (RZ) could be shifted to the HTL/EML interface because of the limited flow of holes as compared to that of electrons. Meanwhile, recombination of free charge carriers in materials with a low mobility is often described by the Langevin recombination rate.[25] Generally, if electron and holes – being

potential recombination partners – wish to recombine, the effective recombination rate is proportional to the "direct" recombination rate or the possibility for finding each other. In high mobility semiconductors, the former is dominant. However, in disordered solids, and particularly disordered organic semiconductors, the low mobility limits the effective recombination rate. The process of finding each other can be described as diffusion limited, which is proportional to the charge carrier mobility as follow:[26]

$$k_{lan} = \frac{q(\mu_e + \mu_h)}{\varepsilon_0 \varepsilon_r}$$

where k_{lan} is the Langevin recombination rate, q is the elementary charge, μ_e is the electron mobility, μ_h is the hole mobility, ε_r is the relative permittivity (≈ 3), and ε_0 is the vaccum permittivity (≈ 8.85 x 10^{-14} F/cm).

For this reason, we can conclude that **3**,**9**-**DCBQ** has the best molecular structure to realize the most desirable device performance because it shows the best electron transporting behavior than the **3**,**6**-**DCP** and **2**,**9**-**DCBQ**. Indeed, the **Device C** showed the highest the current density while **Device A** and **B** showed the similar level of the current density as we commented previously [see also Fig. 6(a)].

Fig. 6(c) shows the normalized EL spectra of **Devices A**-**C** at a brightness of 1000 cd/m^2. All devices exhibited similar EL spectra with a peak wavelength (λ_{max}) at 520 nm.

4. Conclusions

Novel bipolar hosts with benzo[f]quinoline as an electron acceptor moiety were successfully synthesized in high overall yields. They exhibited moderately high glass transition temperatures (> 132 °C) and good thermal stability (Td, > 395 °C). Replacement of the C-3 carbon of phenanthrene by nitrogen facilitated electron transporting behavior which enhances

the charge recombination inside EML. Among the prepared hosts, **3,9-DCBQ** with an asymmetric structure which realizes complete HOMO-LUMO spatial separation showed best EML behavior (i.e., a maximal current efficiency of 48.5 cd/A and a maximal power efficiency of 20.6 lm/W) compared to those of pseudo-symmetrical **3,6-DCP** and **2,9-DCBQ** molecules.

Supplementary data

3D molecular structures and dihedral angles of three hosts. ^{1}H- and ^{13}C-NMR spectra of **3,6-DCP**, **2,9-DCBQ**, and **3,9-DCBQ**.

Acknowledgments

This work was supported by Basic Science Research Program through the National Research Foundation of Korea (NRF) funded by the Ministry of Education (NRF-2015R1D1A3A01020008). This research was also supported by National R&D Program through the National Research Foundation of Korea(NRF) funded by the Ministry of Science & ICT (NRF-2017M3A7B4041701).

References

[1] Son KS, Yahiro M, Imai T, Yoshizaki H, Adachi C. Analyzing Bipolar Carrier Transport Characteristics of Diarylamino-Substituted Heterocyclic Compounds in Organic Light-Emitting Diodes by Probing Electroluminescence Spectra. Chem Mater. 2008;20(13):4439-46.

[2] Su S-J, Sasabe H, Takeda T, Kido J. Pyridine-Containing Bipolar Host Materials for Highly Efficient Blue Phosphorescent OLEDs. Chem Mater. 2008;20(5):1691-3.

[3] Prache O. Active matrix molecular OLED microdisplays. Displays. 2001;22(2):49-56.

[4] Hung W-Y, Chi L-C, Chen W-J, Mondal E, Chou S-H, Wong K-T, et al. A carbazole-phenylbenzimidazole hybrid bipolar universal host for high efficiency RGB and white PhOLEDs with high chromatic stability. J Mater Chem. 2011;21(48):19249-56.

[5] Chou H-H, Cheng C-H. A Highly Efficient Universal Bipolar Host for Blue, Green, and Red Phosphorescent OLEDs. Adv Mater. 2010;22(22):2468-71.

[6] Su S-J, Cai C, Kido J. RGB Phosphorescent Organic Light-Emitting Diodes by Using Host Materials with Heterocyclic Cores: Effect of Nitrogen Atom Orientations. Chem Mater. 2011;23(2):274-84.

[7] Wagner D, Hoffmann ST, Heinemeyer U, Münster I, Köhler A, Strohriegl P. Triazine Based Bipolar Host Materials for Blue Phosphorescent OLEDs. Chem Mater. 2013;25(18):3758-65.

[8] Chen Y-M, Hung W-Y, You H-W, Chaskar A, Ting H-C, Chen H-F, et al. Carbazole-benzimidazole hybrid bipolar host materials for highly efficient green and blue phosphorescent OLEDs. J Mater Chem. 2011;21(38):14971-8.

[9] Zhan X, Sun N, Wu Z, Tu J, Yuan L, Tang X, et al. Polyphenylbenzene as a Platform for

Deep-Blue OLEDs: Aggregation Enhanced Emission and High External Quantum Efficiency of 3.98%. Chem Mater. 2015;27(5):1847-54.

[10] Neogi I, Bajpai A, Savitha G, Moorthy JN. Tetraarylbiphenyl as a New Lattice Inclusion Host by Structure Reductionism: Shape and Size Complementarity Based on Torsional Flexibility. Crystal Growth & Design. 2015;15(5):2129-36.

[11] Marc Veen E, L. Feringa B, M. Postma P, T. Jonkman H, L. Spek A. Solid state organisation of C60 by inclusion crystallisation with triptycenes[dagger]. Chem Commun. 1999(17):1709-10.

[12] Antonioletti R, Bonadies F, Ciammaichella A, Viglianti A. Lithium hydroxide as base in the Wittig reaction. A simple method for olefin synthesis. Tetrahedron. 2008;64(20):4644-8.

[13] Saiyed AS, Patel KN, Kamath BV, Bedekar AV. Synthesis of stilbene analogues by one-pot oxidation-Wittig and oxidation-Wittig–Heck reaction. Tetrahedron Lett. 2012;53(35):4692-6.

[14] Wang H-J, Chen Y-P, Chen Y-C, Chen C-P, Lee R-H, Chan L-H, et al. Synthesis and photovoltaic properties of two-dimensional conjugated polythiophene derivatives presenting conjugated triphenylamine/thiophene moieties. Polymer. 2012;53(19):4091-103.

[15] Babudri F, Cardone A, Cassano T, Farinola GM, Naso F, Tommasi R. Synthesis and optical properties of a poly(2′,5′-dioctyloxy-4,4′,4″- terphenylenevinylene) with high content of (Z) vinylene units. J Organomet Chem. 2008;693(15):2631-6.

[16] Austin M, Egan OJ, Tully R, Pratt AC. Quinoline synthesis: scope and regiochemistry of photocyclisation of substituted benzylidenecyclopentanone O-alkyl and O-acetyloximes. Org Biomol Chem. 2007;5(23):3778-86.

[17] Prajapati SM, Patel KD, Vekariya RH, Panchal SN, Patel HD. Recent advances in the synthesis of quinolines: a review. RSC Advances. 2014;4(47):24463-76.

[18] An X-D, Yu S. Visible-Light-Promoted and One-Pot Synthesis of Phenanthridines and Quinolines from Aldehydes and O-Acyl Hydroxylamine. Org Lett. 2015;17(11):2692-5.

[19] Xie X, Zhang TY, Zhang Z. Synthesis of Bulky and Electron-Rich MOP-type Ligands and Their Applications in Palladium-Catalyzed C−N Bond Formation. J Org Chem. 2006;71(17):6522-9.

[20] Cho MJ, Kim SJ, Yoon SH, Shin J, Hong TR, Kim HJ, et al. New Bipolar Host Materials for Realizing Blue Phosphorescent Organic Light-Emitting Diodes with High Efficiency at

1000 cd/m2. ACS Applied Materials & Interfaces. 2014;6(22):19808-15.

[21] Jiang W, Tang J, Ban X, Sun Y, Duan L, Qiu Y. Ideal Bipolar Host Materials with Bis-benzimidazole Unit for Highly Efficient Solution-Processed Green Electrophosphorescent Devices. Org Lett. 2014;16(20):5346-9.

[22] Jeon SO, Lee JY. Comparison of symmetric and asymmetric bipolar type high triplet energy host materials for deep blue phosphorescent organic light-emitting diodes. J Mater Chem. 2012;22(15):7239-44.

[23] Yook KS, Lee JY. Small Molecule Host Materials for Solution Processed Phosphorescent Organic Light-Emitting Diodes. Adv Mater. 2014;26(25):4218-33.

[24] Lee CW, Lee JY. High Quantum Efficiency in Solution and Vacuum Processed Blue Phosphorescent Organic Light Emitting Diodes Using a Novel Benzofuropyridine-Based Bipolar Host Material. Adv Mater. 2013;25(4):596-600.

[25] Langevin P. Recombination et mobilities des ions dans les gaz. Ann Chim Phys. 1903;28:433.

[26] Burke TM, Sweetnam S, Vandewal K, McGehee MD. Beyond Langevin Recombination: How Equilibrium Between Free Carriers and Charge Transfer States Determines the Open-Circuit Voltage of Organic Solar Cells. Adv Energy Mater. 2015;5(11):1500123.

FIG. CAPTIONS

Scheme 1. Syntheses of three hosts

Fig. 1. HOMO and LUMO energies of phenantherene and its nitrogen-containing analogues calculated by DFT/B3LYP.

Fig. 2. UV-visible absorption and PL spectra of (a) **3,6-DCP**, (b) **2,9-DCBQ**, and (c) **3,9-DCBQ**.

Fig. 3. (a) DSC and (b) TGA curves of **3,6-DCP**, **2,9-DCBQ**, and **3,9-DCBQ**.

Fig. 4. Optimized molecular geometries of (a) **3,6-DCP**, (b) **2,9-DCBQ**, and (c) **3,9-DCBQ** showing LUMOs (left), HOMOs (middle), and side views (right).

Fig. 5. Energy diagrams of three green PHOLEDs.

Fig. 6. (a) current density-voltage-luminance curves, (b) current and external quantum efficiencies, (c) normalized electroluminescence spectra of fabricated green PHOLEDs (at a brightness of 1,000 cd/m^2).

Scheme 1. Syntheses of three hosts

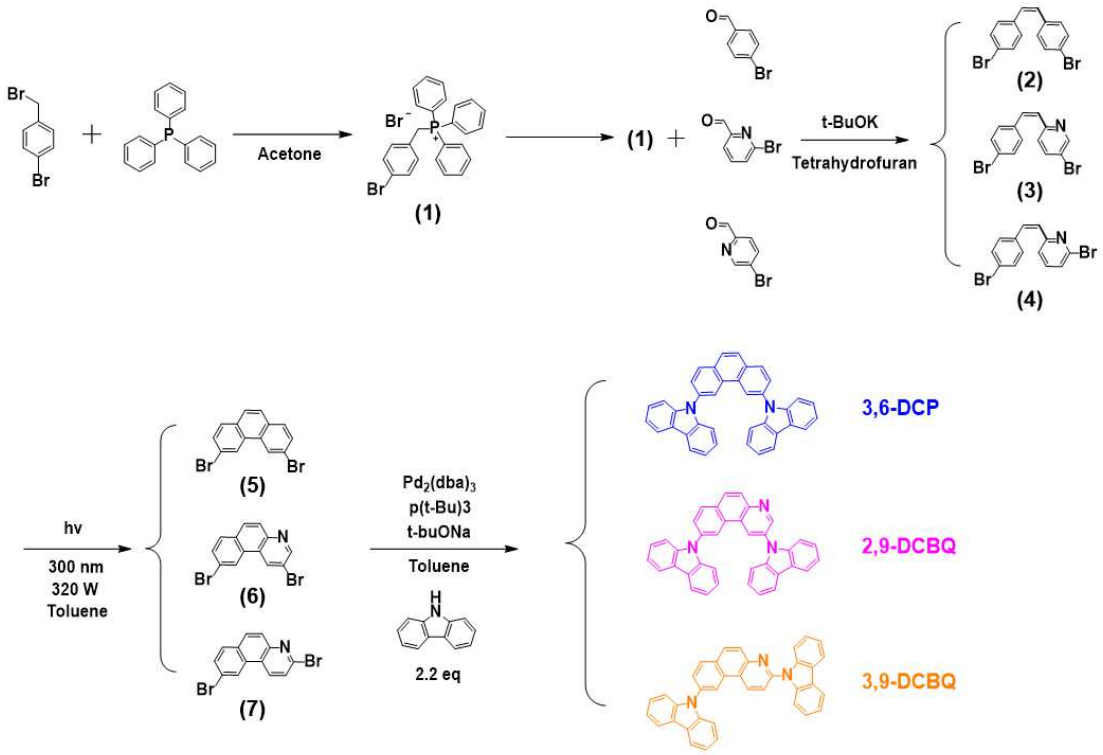

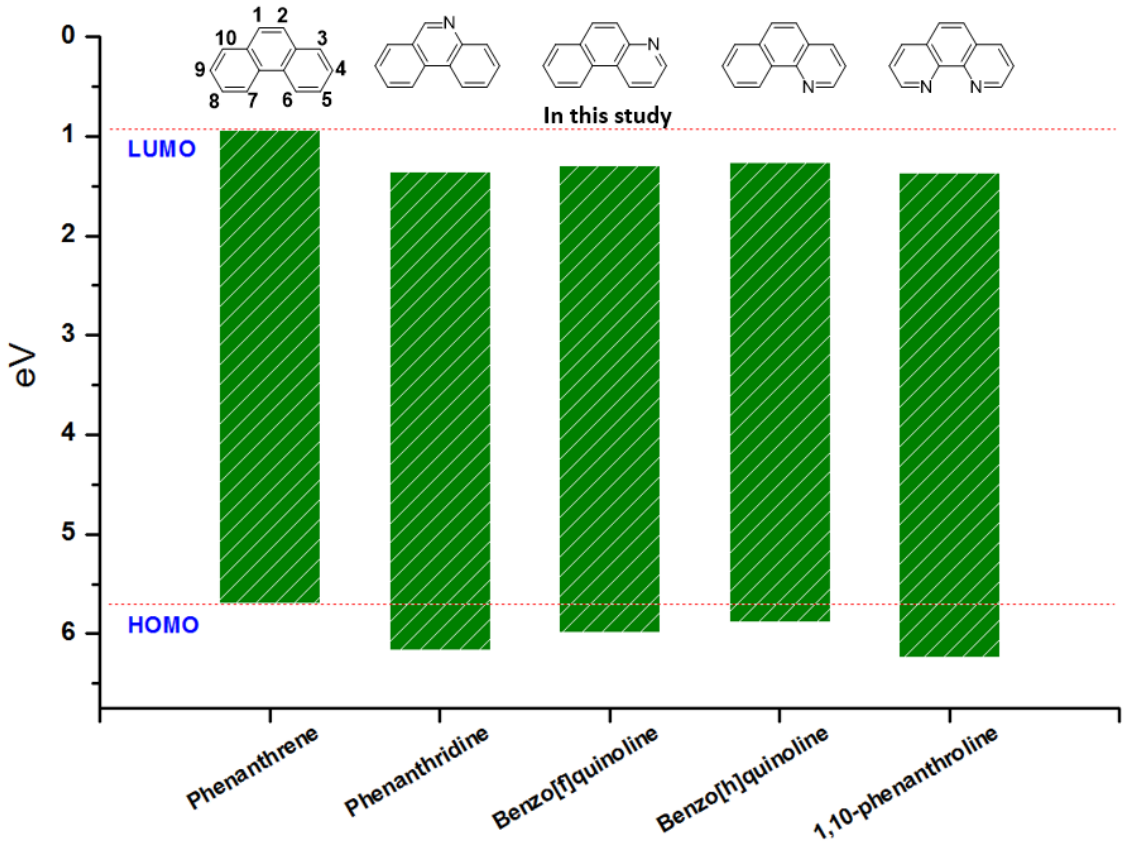

Fig. 1. HOMO and LUMO energies of phenantherene and its nitrogen-containing analogues calculated by DFT/B3LYP.

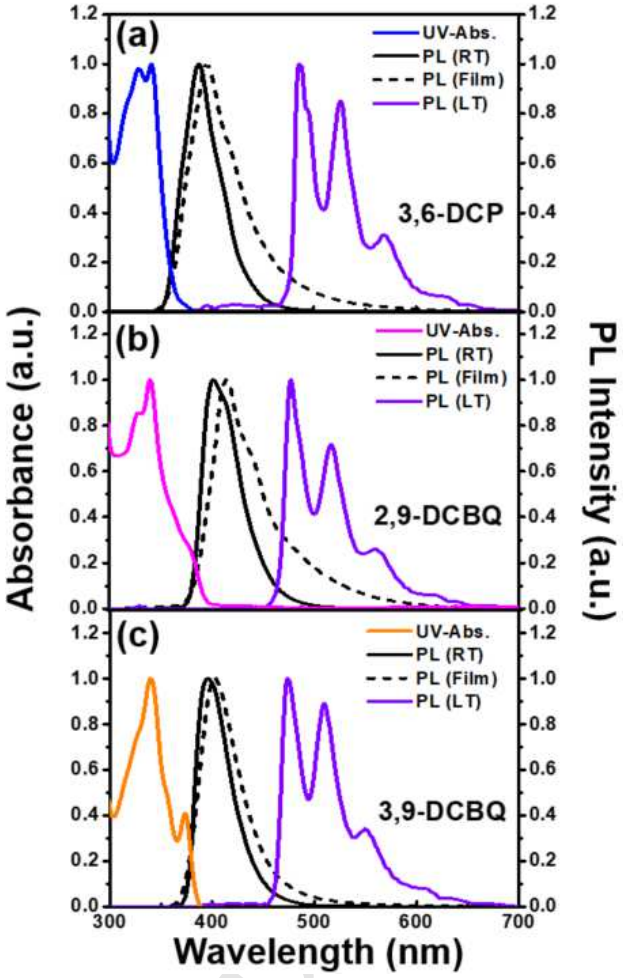

Fig. 2. UV-visible absorption and PL spectra of (a) **3,6-DCP**, (b) **2,9-DCBQ**, and (c) **3,9-DCBQ**.

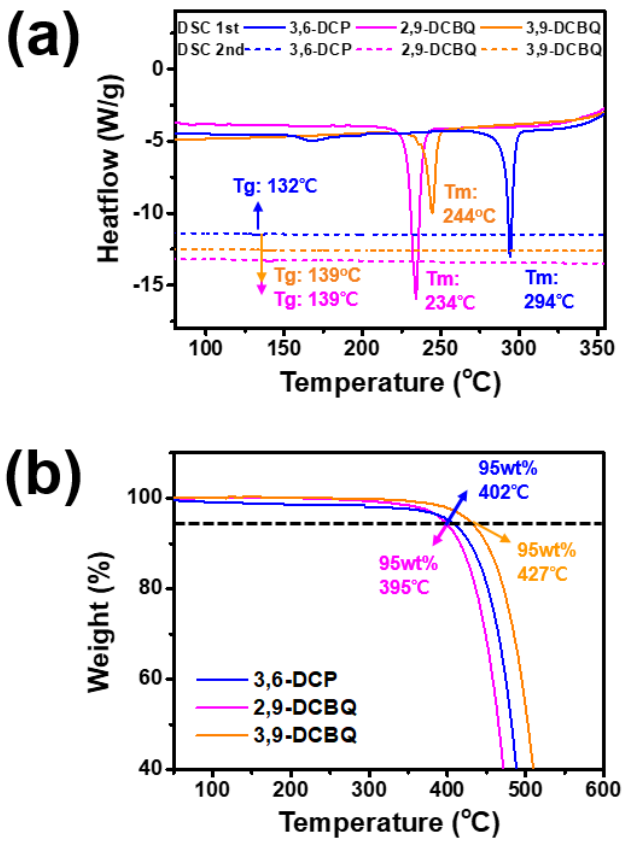

Fig. 3. (a) DSC and (b) TGA curves of **3,6-DCP**, **2,9-DCBQ**, and **3,9-DCBQ**.

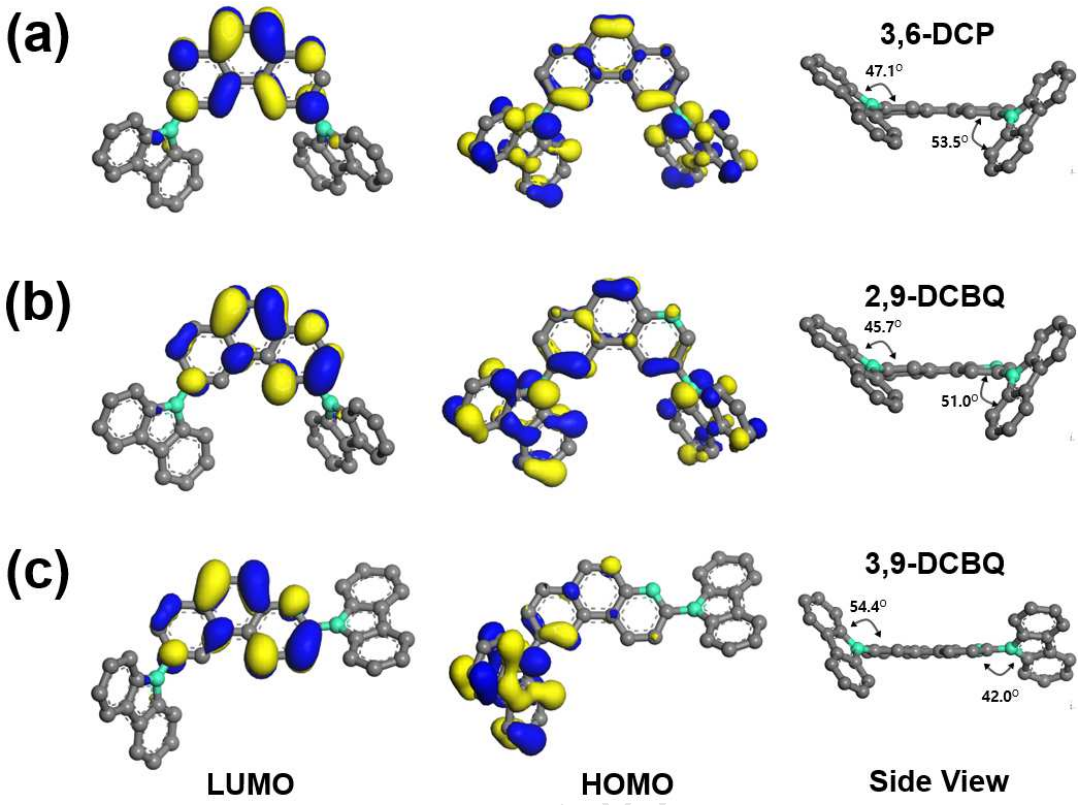

Fig. 4. Optimized molecular geometries of (a) **3,6-DCP**, (b) **2,9-DCBQ**, and (c) **3,9-DCBQ** showing LUMOs (left), HOMOs (middle), and side views (right).

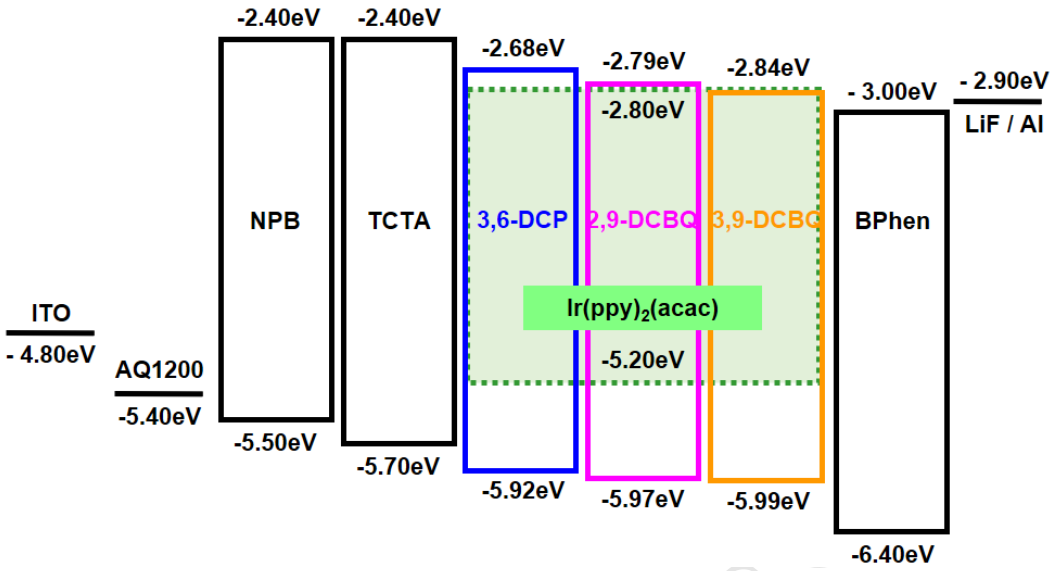

Fig. 5. Energy diagrams of three green PHOLEDs.

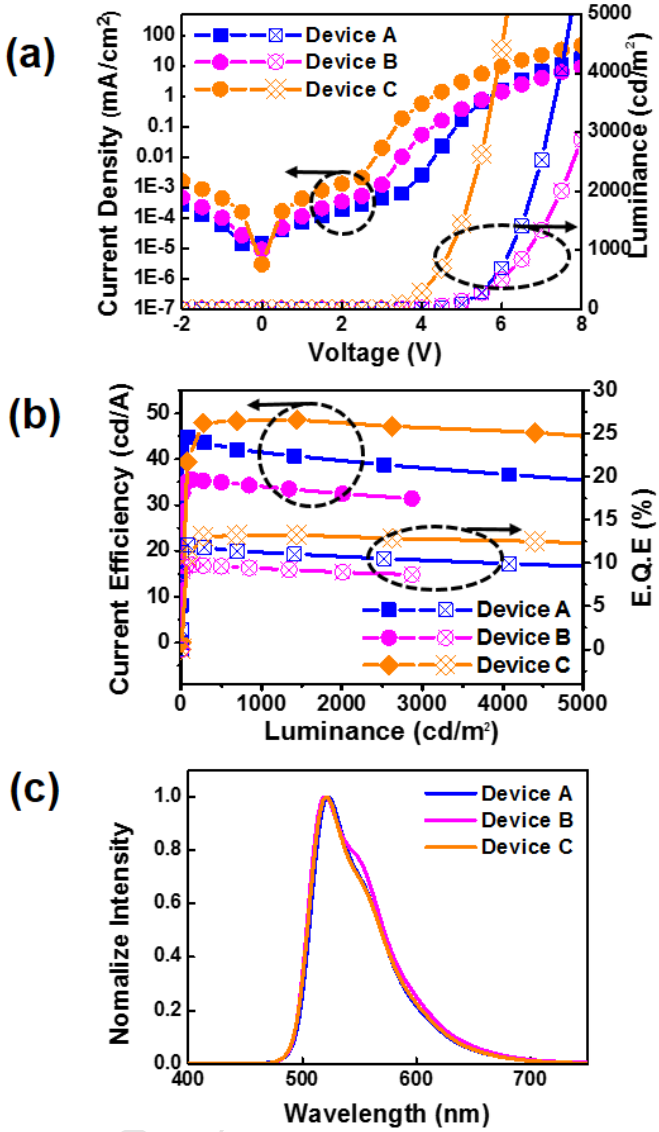

Fig. 6. (a) current density-voltage-luminance curves, (b) current and external quantum efficiencies, (c) normalized electroluminescence spectra of fabricated green PHOLEDs (at a brightness of 1,000 cd/m^2).

Table 1. Photophysical, thermal, electrochemical properties of green host materials

Compound	Solution [nm][a]		Film [nm]		T_g [°C]	T_m [°C]	T_d [°C]	HOMO [eV][b]	LUMO [eV][c]	E_g [eV][d]	E_T [eV]
	λ_{abs}	λ_{em}	λ_{abs}	λ_{em}							
3,6-DCP	329, 340	388	335, 347	395	132	294	402	–5.92	–2.68	3.24	2.56
2,9-DCBQ	329, 340	401	344	414	139	234	395	–5.97	–2.79	3.18	2.60
3,9-DCBQ	340, 374	396	344, 377	402	139	244	427	–5.99	–2.84	3.15	2.62

[a]Maximum absorption and emission wavelengths measured in toluene solution (~1×10^{-5} M). [b]HOMO = $-(4.8\ \text{eV} + E_{ox}^{onset})$. [c]LUMO = E_g^{opt} + HOMO [d]Optical band gap estimated from the absorption edge (λ_{edge}) in solution as $E_g = 1240/\lambda_{edge}$.

Table 2. Summary of device characteristics of the green PHOLEDs

Device	V_{on}[a)]/V_{op}[b)] [V]	CE[c)]/PE[d)]/EQE[e)] [$cdA^{-1}/lmW^{-1}/\%$]		CIE[f)] (x,y)
		Maximum	At 1000cd m^{-2}	
Device A	4.2/6.1	44.0/13.1/12.1	42.0/12.3/11.4	(0.33,0.62)
Device B	3.5/6.6	35.5/12.3/9.8	34.3/11.2/9.4	(0.32, 0.62)
Device C	3.0/4.7	48.5/20.6/14.3	48.3/19.4/13.1	(0.33, 0.62)

[a] V_{on}: turn-on voltage, measured at 1 cd m^{-2} [b] V_{op}: operating voltage, measured at 1000 cd m^{-2} [c] CE: current efficiency [d] PE: power efficiency [e] EQE: external quantum efficiency, The EQE was obtained from the calculation based on the assumption of a Lambertian distribution [f] CIE: Commission International de L'Eclairage.

Graphic Abstract

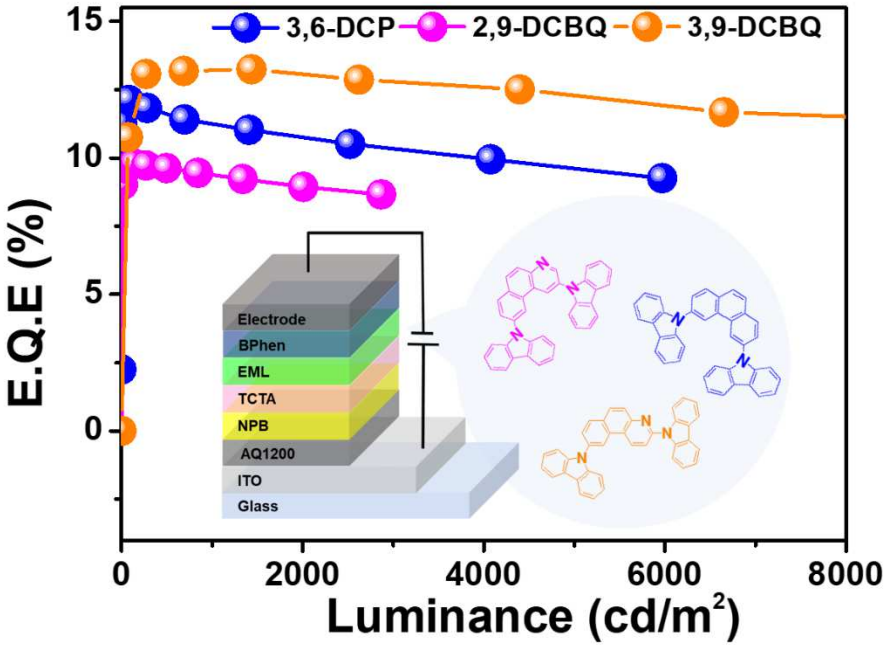

Highlights

> High overall yields over four synthetic steps equaling ~48%.
> Bipolar properties originated from carbazole and benzo[f]quinoline moieties.
> High thermal stability and asymmetric molecular structure with complete HOMO-LUMO spatial separation